

# Mutual Information as a Figure of Merit for Optical Fiber Systems

Tobias Fehenberger, *Student Member, IEEE* and Norbert Hanik, *Senior Member, IEEE*

**Abstract**—Advanced channel decoders rely on soft-decision decoder inputs for which mutual information (MI) is the natural figure of merit. In this paper, we analyze an optical fiber system by evaluating MI as the maximum achievable rate of transmission of such a system. MI is estimated by means of histograms for which the correct bin number is determined in a blind way. The MI estimate obtained this way shows excellent accuracy in comparison with the true MI of 16-state quadrature amplitude modulation (QAM) over an additive white Gaussian noise channel with additional phase noise, which is a simplified model of a nonlinear optical fiber channel. We thereby justify to use the MI estimation method to accurately estimate the MI of an optical fiber system. In the second part of this work, a transoceanic fiber system with 6000 km of standard single-mode fiber is simulated and its MI determined. Among rectangular QAMs, 16-QAM is found to be the optimal modulation scheme for this link as to performance in terms of MI and requirements on components and digital signal processing. For the reported MI of 3.1 bits/symbol, a minimum coding overhead of 29% is required when the channel memory is not taken into account. By employing ideal single-channel digital back-propagation, an increase in MI by 0.25 bits/symbol and 0.28 bits/symbol is reported for 16-QAM and 64-QAM, respectively, lowering the required overhead to 19% and 16%. When the channel spacing is decreased to be close to the Nyquist rate, the dual-polarization spectral efficiency is 5.7 bits/s/Hz, an increase of more than 2 bits/symbol compared to a 50 GHz spacing.

**Index Terms**—Mutual information, achievable rate, channel coding, long-haul fiber communication, digital back-propagation

## I. INTRODUCTION

THE demand for increased data rates in optical long-haul communications has been growing for several years. A capacity crunch [1] seems inevitable and spatial multiplexing is considered by many as the only solution to this problem because it offers lower costs due to integration of components [2]. The investment costs to deploy new fibers, however, are high and spatially multiplexed systems have not reached a commercial level for long-haul fiber communication. Hence, optical networks operators rely for the time being on currently deployed single-mode fibers instead of switching to new fiber technologies. For those single-mode fibers, an obvious improvement on the de-facto standard long-haul 100 Gbit/s/channel systems operating with quadrature phase-shift keying (QPSK) at 28 billion symbols per second per polarization can be made by increasing the order of the modulation scheme. The accompanying increased susceptibility

to noise is in conflict to the requirement that the bit error ratio (BER) after decoding (denoted  $\text{BER}_{\text{out}}$ ) must be kept at a constant level of around  $10^{-15}$  and that the transmission distance must remain the same. The required protection of bits can be achieved on the information-theoretic layer by applying more advanced coding schemes. Most of these schemes have a decoder that operates with soft inputs, offering an improved decoding threshold because the reliability of a bit decision is taken into account. As we will outline in detail in Section II, using mutual information (MI) as a figure of merit is more natural to this family of soft-decision decoders. More importantly for this work, it also lets us determine the maximum achievable rate of an optical fiber channel.

MI has been a key quantity in the field of information theory since Shannon's seminal paper [3]. In optical communications, it has been used to state lower-bound estimates on channel capacity [4], [5]. Recently, MI has drawn attention as an forward error correction (FEC) decoding threshold. Optical transmission experiments [6] suggest that MI is more reliable than the  $Q^2$  factor in order to estimate the post-decoding BER of a particular soft-decision (SD) decoder. MI predicting the BER after decoding has also been applied in simulations to long-haul links [7]. It is also used as decoding threshold in record experiments [8]. When MI represents a decoding threshold, it is calculated from bit-wise log-likelihood ratios (LLRs) representing the soft a-priori information coming from the channel to the decoder. To calculate LLRs, a distribution of the received symbols must be assumed. Typically, the noise is taken to be Gaussian, although this assumption does not always hold in optical communications [9].

In this work we do not make any assumptions on the noise characteristics of an optical channel. Instead, MI is estimated by means of histograms for which the correct number of bins is determined with a blind and accurate method. When applied to an optical fiber link, MI is used to find the maximum potential data throughput over a fiber. Further, MI serves as a relative figure of merit to assess the impact of changing a design parameter or adding a routine to the receiver with respect to achievable rate. This analysis is performed exemplarily by employing digital back-propagation (DBP) and for varying spectral channel spacings.

This paper is organized as follows. Section II explains information-theoretic fundamentals of channel coding and introduces a reference channel model. In Section III, a method for MI estimation is presented and its accuracy verified. Simulating an optical transmission system and applying MI to it is outlined in Section IV. Section V concludes this work.

T. Fehenberger and N. Hanik are with the Institute for Communications Engineering, Technische Universität München, 80333 Munich, Germany (E-mail: tobias.fehenberger@tum.de, norbert.hanik@tum.de).

## II. INFORMATION THEORY

### A. Hard and Soft Decisions

Every code consists of at least two entities, an encoder that maps bits to codewords and a corresponding decoder that tries to undo this mapping when only a distorted copy of the sent codeword is available at the decoder. The input into such a decoder can be hard-decision (HD) or SD, depending on the design of the symbol demapper and the code. For simplicity, we will refer to codes whose decoders use soft (hard) input as SD (HD) codes. Note that there are code families that work with both hard and soft decoding. See for example [10] on how SD decoding is applied to Reed-Solomon (RS) codes.

For hard decisions, the binary sequence after the demapper is quantized such that all information available at the decoder input is binary. In contrast, SD decoding operates with more than two quantization levels. The reliability of a received symbol with respect to the decoder operation is increased by taking into account the distance of a symbol to its decision boundaries. The closer a symbol is to the decision region of a different symbol, the less reliable the decision on this symbol is going to be. With an infinite number of quantization levels, it can be shown [11, Sec. 6.8] that SD decoding outperforms HD codes by up to 2 dB of energy per bit for the code rate  $R \rightarrow 0$ . For a practical rate up to about 0.9, the potential gain is still larger than 1 dB. Hence, even the most powerful HD codes are outperformed by SD codes.

For many years, HD codes such as the ubiquitous RS code with  $K = 8 \cdot 239$  information bits per block of length  $N = 8 \cdot 255$  bits [12] have been the most prominent coding schemes in optical long-haul systems. Improved FEC for optical communications [13] is mostly based on hard decisions as well. The focus on HD codes can be mainly attributed to two of their characteristics. Firstly the computational complexity is small because computations are made with integers rather than floating points. Additionally, it is possible to exactly determine the decoding performance by solely considering the BER at the decoder input (denoted  $\text{BER}_{\text{in}}$ ) when perfect interleaving is assumed. For the RS (255, 239) code of rate  $R = K/N = 239/255$  (which corresponds to a coding overhead of  $(1/R) - 1 \simeq 6.7\%$ ), the  $\text{BER}_{\text{in}}$  must be around  $8.3 \cdot 10^{-5}$  in order to reach a  $\text{BER}_{\text{out}}$  of  $10^{-15}$  [12]. Further improvements on HD code design allow the  $\text{BER}_{\text{in}}$  to go as high as  $4.64 \cdot 10^{-3}$  [14] for a coding overhead of 6.7% and a  $\text{BER}_{\text{out}}$  of less than  $10^{-15}$ . This so-called FEC decoding threshold is usually stated in terms of the  $Q^2$  factor, which is defined as

$$Q^2 = 20 \log_{10}(\sqrt{2} \cdot \text{erfc}^{-1}(2 \cdot \text{BER}_{\text{in}})) \quad \text{in dB}, \quad (1)$$

where  $\text{erfc}^{-1}$  denotes the inverse of the complementary error function.  $Q^2$  is thus a perfectly suitable figure of merit for an HD code if the  $\text{BER}_{\text{out}}$  is to be examined. Unfortunately, this one-to-one correspondence between  $\text{BER}_{\text{in}}$  (or equivalently  $Q^2$ ) and  $\text{BER}_{\text{out}}$  is not given for most SD codes. It is in general impossible to analytically determine the decoding performance of an SD code with finite block-length by considering an input at the decoder. For most SD coding schemes, the decoding operation starts with soft a-priori information from

the channel, usually in the form of LLRs.  $\text{BER}_{\text{in}}$  does not play a role at the decoder input and it consequently makes no sense to cling to  $Q^2$  as a figure of merit for these codes. Instead of using  $Q^2$  as characteristic prediction for  $\text{BER}_{\text{out}}$ , MI is the more natural and also more robust figure of merit [6].

In addition, MI enables us to evaluate the influence of certain design parameters in terms of net achievable rate. We will illustrate this with a short example. Consider a nonlinear, wavelength-division multiplexed (WDM) optical communication link with either an HD or an SD coding scheme in place. For this system the influence of increasing the WDM channel spacing is to be examined. We expect the signal quality in general to improve for an increased spacing because the impact of nonlinear signal-signal interactions is weaker. For the HD code, the improvement from increasing the spectral spacing translates to an increased  $Q^2$  and consequently a smaller  $\text{BER}_{\text{out}}$  that can be calculated analytically. If the required  $\text{BER}_{\text{out}}$  is already reached, the improvement due to larger WDM spacing essentially corresponds to an assured gain in link budget. In contrast, a gain in  $Q^2$  does not translate to any characteristic of an SD decoder. Most importantly, not even a lower  $\text{BER}_{\text{out}}$  can be guaranteed. Let us now consider the SD code and MI as figure of merit at its decoder input. Similarly to the previous HD case, MI grows with increasing channel spacing. Let us also assume a capacity-achieving code with perfectly flexible coding rate. These assumptions are fulfilled by spatially-coupled low-density parity-check (LDPC) codes [15] and polar codes [16]. Both coding schemes provably achieve the capacity of an additive white Gaussian noise (AWGN) channel while maintaining low decoding complexity. Polar codes further offer a perfectly flexible rate by using the  $K$  best polarized sub-channels. Exploiting these properties, we can use the gain in MI to lower the rate of the used SD code such that we operate right at the achievable rate. A change in MI hence directly translates to change in net available data rate. In the following, we elaborate on this concept. We also show simulation results for the presented example in Section IV-B.

### B. Channel Capacity, Mutual Information, Achievable Rate

Consider two random variables  $X$  and  $Y$  representing the channel input and output, respectively. Shannon [3, Sec. 12] tells us that the capacity of a channel is the maximum rate of transmission, or equivalently, the MI  $I(X; Y)$  maximized over all possible input distributions  $p_X$ ,

$$C = \max_{p_X} I(X; Y). \quad (2)$$

The MI  $I(X; Y)$  represents the amount of information about  $X$  that is contained in  $Y$  when  $X$  is transmitted. It is also the achievable rate, i.e. the rate for which the BER tends to zero as the block length of the code goes to infinity. Rates that are smaller than the channel capacity yield an arbitrarily small BER when the block length is sufficiently large [17, Sec. 7.6]. For practical applications, restrictions are made to the channel input and output. The channel input  $X$  is fixed to a certain modulation format, which is required to map information onto the symbols at the transmitter. Hence,  $X$  is a fixed discrete

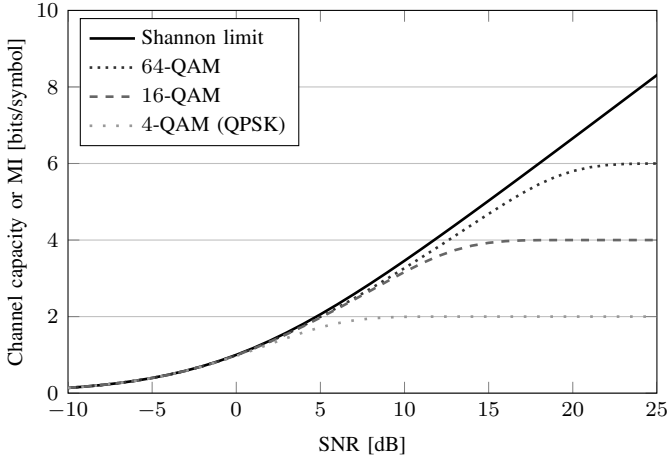


Fig. 1. Circularly symmetric AWGN channel capacity (Shannon limit) and MI of QAM of order 4, 16, 64 over this channel.

random variable with alphabet  $\mathcal{X}$  whose cardinality  $|\mathcal{X}|$  is the modulation order  $M$ . In this work, we further assume the input distribution  $p_X$  to be uniformly distributed. The channel output  $Y$  is also discrete, which is motivated by using an analog-to-digital converter (ADC) at the receiver. Under these assumptions, the MI is (see for example [18, Sec. 23.2])

$$I(X; Y) = \sum_{m=1}^M \sum_{y \in \mathcal{Y}} p_X(x_m) p_{Y|X}(y|x_m) \log_2 \left[ \frac{p_{Y|X}(y|x_m)}{p_Y(y)} \right], \quad (3)$$

where  $p_{Y|X}(y|x_m)$  is a conditional probability mass function (pmf) of an output realization  $y \in \mathcal{Y}$  given the  $m^{\text{th}}$  input realization  $x_m \in \mathcal{X}$  and  $p_Y(y)$  is the pmf of the output. The second sum represents summing over all values of  $\mathcal{Y}$  in the complex domain. For a uniformly distributed input,  $p_X(x) = \frac{1}{M}$ .

An important aspect of the optical channel is its inherent memory. In this work, we neglect any memory and do not make use of the statistical relations between neighboring symbols. Thereby, a memoryless auxiliary channel is introduced. The MI of this auxiliary channel is proven to be a lower bound of the MI of the true channel with memory [19, Sec. VI]. This means that the MI of the auxiliary channel is still an achievable rate. This relation between MI and achievable rate serves as basis for the analysis carried out in Section IV.

For a complex cs AWGN channel, whose noise distributions along the two complex dimensions are independent, the capacity-achieving distribution under an average-power constraint is continuous complex Gaussian. Its channel capacity is given by the well-known formula  $C = \log_2(1 + \text{SNR})$ . This quantity as well as the MI of quadrature amplitude modulation (QAM) of respective order  $M = \{4, 16, 64\}$  transmitted over this channel are shown in Fig. 1 as a function of signal-to-noise ratio (SNR) in dB. Among the many important features to be seen in Fig. 1, we want to point out that the MI of each discrete modulation format saturates at a maximum of  $\log_2 M$  bits/symbol for high SNRs. Also, the MI for all depicted modulation schemes is approximately the same in the low-to-medium SNR regime.

### C. Reference Channel Model

Estimating the optical fiber capacity, or at least lower bounds thereof, has been a vivid research topic for several years [4] [5]. So far, no explicit capacity expression is known as there is no analytical channel model for a dispersive nonlinear fiber channel with inline amplification. However, several approximate channel models exist that simplify the noise distributions of the optical channel by making certain assumptions. Among these models, the Gaussian noise model [20], the partially coherent AWGN (p.c. AWGN) model [21], [22] and an input-dependent complex AWGN model with non-diagonal covariance matrix [9] have received notable attention. The latter model will not be considered further as it models the orientation of the received ellipse-shaped constellation symbols in dependence of the channel input, which is not suitable for our analysis. In this work, we use the p.c. AWGN channel as reference. The time-discrete form of the p.c. AWGN channel is [21]

$$Y = X \cdot e^{j\Phi} + N, \quad (4)$$

where the additive noise  $N$  is a complex Gaussian-distributed random variable with zero mean and noise power spectral density  $\frac{N_0}{2}$  per complex dimension,  $N \sim \mathcal{N}(0, N_0)$ .  $\Phi$  models the phase noise as real-valued wrapped AWGN with variance  $\sigma_\Phi^2$ . The well-known AWGN channel is thus a special case of (4) with  $\sigma_\Phi^2 = 0$ . The p.c. AWGN channel is essentially a circularly symmetric (c. s.) AWGN channel with additional phase noise such that in the absence of AWGN, excessive phase noise leaves only the amplitude to transmit information. This makes the channel only *partially* usable to convey information, hence its name [21]. As a simplified approximation to a nonlinear channel, the additional phase noise models nonlinearities due to the Kerr effect as well as residual linear impairments that are not fully compensated at the receiver. A higher optical transmit power resulting in more nonlinearities, an or insufficient linear compensation at the receiver lead to an increase in phase noise. The p.c. AWGN channel exhibits the typical concave function of channel capacity estimate over optical launch power, known from e.g. [4], if for increasing signal power the phase noise is modeled such that it grows faster than the signal power. The nonlinear regime in optical transmission is approximately represented by  $\sigma_\Phi^2$  less than  $10^{-1}$  [22].

The transition probability density function (pdf) of the p.c. AWGN channel (4) is obtained by combining the pdf of a real-valued wrapped Gaussian random variable and the pdf of complex AWGN [22],

$$p_{Y|X}(y|x) = \int_{-\pi}^{+\pi} \frac{1}{\pi N_0} e^{-\frac{|y-xe^{j\varphi}|^2}{N_0}} \cdot \frac{1}{\sqrt{2\pi\sigma_\Phi^2}} \sum_{k=-\infty}^{+\infty} e^{-\frac{(\varphi-2\pi k)^2}{2\sigma_\Phi^2}} d\varphi. \quad (5)$$

This pdf fully describes the relation between channel input  $X$  and output  $Y$ . When the input  $X$  is known at the receiver, the MI  $I(X; Y)$  of (3) can be calculated. This is done in Section III-C to obtain a MI reference for the MI estimate that is obtained with the method presented in the following.

### III. ESTIMATING MUTUAL INFORMATION

If the pdfs  $p_{Y|X}(y|x_m)$  and  $p_Y(y)$  of (3) are not known or cannot be stated explicitly for the channel of interest, MI cannot be determined numerically but must be estimated. As MI between random variables is such a fundamental quantity, its estimation is an important research topic not only in information theory but also in, e.g., genetics [23] and neural computation [24]. Accordingly, a lot of known techniques to estimate MI are known, such as B-spline functions [23], kernel density evolution [25], Gauss–Hermite quadratures [26, Sec. III], second-order Taylor expansion [27], nearest neighbor statistics [28], and histograms [29]. Among them, MI estimation by means of histograms is considered in detail in this work as histograms are the conceptually most intuitive and also most straightforward technique to implement. A comparison of different techniques is beyond the scope of this work as the main focus is to find an accurate estimation technique and then apply this method to an optical fiber system.

#### A. Histograms

The principle of histograms is to divide the value range of the symbols  $\mathbf{S}$  into a number of intervals called bins. The number of symbols falling into each bin represents the value of the discrete distribution when apt normalization is performed. Correctly choosing the number of bins is crucial to obtain an estimate of the pdfs and thus of MI that is as exact as possible. For too few bins, the estimate becomes too coarse and does not accurately resemble the distribution. If the number of bins is chosen too large, MI tends to be overestimated. This is because MI estimation is based on a sequence of finite length. Using a large number of bins, there are bins into which no received symbols fall, especially at the low-probability tails of the distribution to be estimated. These tails are usually the portion of the continuous pdf  $p_{Y|X}(y|x_m)$  that overlaps into the decision region of a different sent symbol  $x_{k \neq m}$ . The corresponding summands of this overlap region can be negative for  $\log_2 \left[ \frac{p_{Y|X}(y|x_m)}{p_Y(y)} \right] < 0$  in (3), and  $I(X;Y)$  is decreased by them. If, however, no symbol falls into these bins, they must be excluded from the calculation as the  $\log_2$  in (3) is not defined when either the numerator or the denominator equals zero. This means that terms that reduce the MI are wrongfully left out if we do not take care to produce as few empty bins as possible while recreating the shape of the distribution as good as possible.

To illustrate the effect of using an overly coarse or fine histogram, Fig. 2 depicts the MI over SNR for  $2^{14}$  QPSK symbols transmitted over a c. s. AWGN channel. The MI estimate is obtained with a joint histogram of in-phase and quadrature. The vertical arrow indicates increasing bin number, from 2 bins up to 500 bins per dimension. A too small number of bins leads to an incorrectly small MI estimate. Contrarily, too many bins result in overestimating the actual MI by far. Note that it seems as if there were a certain constant bin number that provided sufficient estimation accuracy. Correctly applying a histogram, however, depends not only on the pdf shape but also on the number of symbols that are evaluated jointly. The more samples are considered for one particular

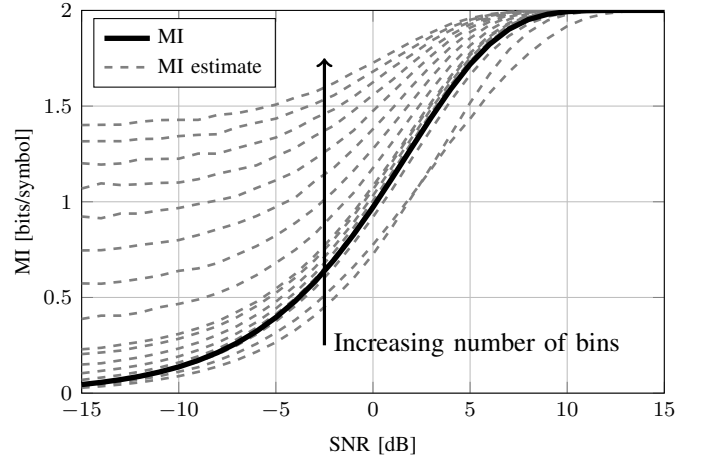


Fig. 2. Numerically calculated MI and MI estimates obtained with histograms of different bin sizes for QPSK over a c. s. AWGN channel. The direction of the arrow indicates increasing number of bins.

instance of a histogram, the more likely it is that symbols fall into the low-probability tails of the pmf and the histogram must be chosen finer. In the following, a method is presented that allows us to calculate the bin number for which we obtain an accurate MI estimation while taking into account the dependence on both the pdf shape and the sequence length.

#### B. Find the Correct Number of Bins

Finding the right number of bins for a histogram is a well-known task, see for example [29], [30], [31], [32]. In this work, the input into the MI estimation algorithm is two-dimensional. Also, we require the pdf estimation to be blind, i.e. only the received symbols may have an impact of the MI estimate. Any a-priori knowledge of the channel characteristics or choosing suitable algorithm parameters should not be required in order not to influence the results by making assumptions.

[30] is proven to be optimal for one-dimensional normally distributed data, which does not match the properties of the communication system at hand. The method presented in [29] is suitable for multi-dimensional data. However, certain parameters for the estimator function must be chosen in order for the algorithm to work, which makes the method not blind. For two-dimensional data, [31] optimizes over both dimensions but gives the same bin number for in-phase and quadrature. The resulting square bins are not optimal for noise that is not symmetrical as it is the case in highly nonlinear fiber optics. Although there might be many more promising techniques, the method presented in [32] is chosen because it is blind and also expandable to two dimensions in an easy manner. We will see in Section III-C that MI estimation using this method is accurate for the p.c. AWGN channel (our reference channel). Finding a potentially superior method is left for future work.

The method described in detail in [32] is based on the idea that a histogram is a piecewise-constant density model of the pdf to be estimated. This allows to state the posterior probability of the bin numbers given a sequence of symbols  $\mathbf{S}$  of length  $N_s$ . The pair of bin numbers of the in-phase and quadrature component is found jointly over both dimensions

and denoted as  $(\hat{N}_{b,\mathcal{I}}, \hat{N}_{b,\mathcal{Q}})$ . For the ease of notation, the product  $N_{b,\mathcal{I}} \cdot N_{b,\mathcal{Q}}$  is written as  $N_b^*$ . [32] states that

$$(\hat{N}_{b,\mathcal{I}}, \hat{N}_{b,\mathcal{Q}}) = \arg \max_{N_{b,\mathcal{I}}, N_{b,\mathcal{Q}}} \left\{ N_s \ln N_b^* + \ln \Gamma\left(\frac{N_b^*}{2}\right) - N_b^* \cdot K + \right. \\ \left. - \ln \Gamma\left(N_s + \frac{N_b^*}{2}\right) + \sum_{k=1}^{N_{b,\mathcal{I}}} \sum_{l=1}^{N_{b,\mathcal{Q}}} \ln \Gamma\left(n_{k,l} + \frac{1}{2}\right) \right\}, \quad (6)$$

where  $\Gamma(x)$  denotes the Gamma function defined as  $\Gamma(x) = \int_0^\infty e^{-t} t^{x-1} dt$  and  $K = \ln \Gamma(\frac{1}{2})$  is a constant. When a histogram operation with  $(N_{b,\mathcal{I}}, N_{b,\mathcal{Q}})$  bins is applied to the symbols  $\mathbf{S}$ , the number of samples falling into the  $k^{\text{th}}$  and  $l^{\text{th}}$  bin along the real and imaginary dimension, respectively, is denoted  $n_{k,l}$ .

The maximization in (6) is solved numerically with a brute-force approach for 1 to  $N_{b,\max}$  bins per dimension. For a reasonably large  $N_{b,\max}$ , the results of Fig. 2, the following simulation results and [32] suggest that an argument that maximizes (6) will not be found by probing more than  $N_{b,\max}$  bins. This limits the computational time of finding the correct bin numbers.

For a block of symbols  $\mathbf{S}$ , the corresponding MI is calculated at the receiver as follows.

- 1) Determine  $(\hat{N}_{b,\mathcal{I}}, \hat{N}_{b,\mathcal{Q}})$  according to (6).
- 2) Perform a two-dimensional histogram operation with  $(\hat{N}_{b,\mathcal{I}}, \hat{N}_{b,\mathcal{Q}})$  bins on  $\mathbf{S}$ . Obtain  $p_Y(y)$  by dividing the number of symbols falling into every bin by  $N_s$ .
- 3) Store the bin positions of step 2.
- 4) Determine  $p_{Y|X}(y|x_m)$  by performing another histogram with the bin positions stored in step 3 on those of the symbols  $\mathbf{S}$  that belong to the  $m^{\text{th}}$  symbol. After normalization,  $p_{Y|X}(y|x_m)$  is obtained.
- 5) Repeat step 4 for every  $m$  from 1 to  $M$ .
- 6) Calculate the MI according to (3).

### C. Numerical Verification

To verify the accuracy of the method, we compare the MI estimate obtained with the presented method to the MI of 16-QAM for a p.c. AWGN channel. The MI is numerically calculated for a given modulation format and noise variances as described in [33]. MI and its respective estimate are depicted in Fig. 3 for 16-QAM, varying SNR values of the additive noise component  $N$  of (4) from  $-5$  dB to 25 dB and a phase noise variance  $\sigma_\Phi^2$  between 0 (c. s. AWGN) and 0.1. Higher values of  $\sigma_\Phi^2$  were omitted because of their practical insignificance. The MI estimate shown in Fig. 3 is very accurate over all simulated additive SNRs and for all values of  $\sigma_\Phi^2$ . For a very small overall noise contribution, the curves are even hardly distinguishable, showing an excellent match between our estimate and the true MI. Further simulations have shown that similar accuracy is obtained for rectangular QAM with  $M$  up to 64.

We conclude that the MI estimation method is sufficiently accurate to determine the MI for rectangular QAM and transmission over a p.c. AWGN channel. As this channel is a valid approximation for an optical fiber channel, it is justified to use our method to obtain an estimate of the MI of an optical communication system.

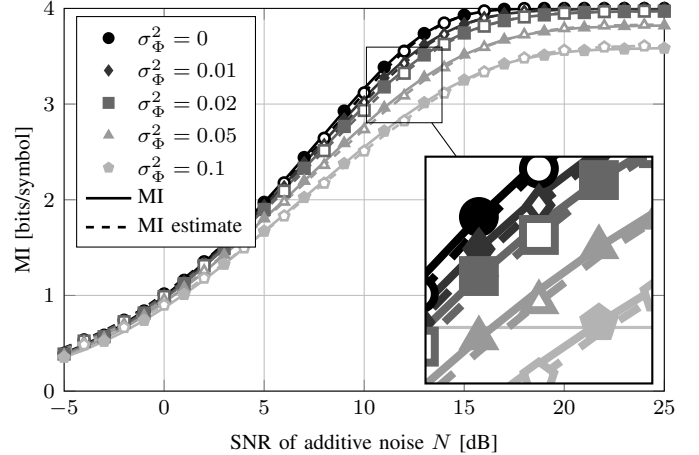


Fig. 3. Numerically calculated MI and MI estimates for 16-QAM, varying additive SNR in dB and  $\sigma_\Phi^2$  from 0 to 0.1.

## IV. FIBER SIMULATIONS

In this section, we describe the simulation setup of an optical communication system. The transmission of QAM symbols is simulated and MI is estimated with the method presented in Section III.

### A. Simulation Setup

A block diagram of the simulation setup is depicted in Fig. 4. The default transmission and fiber link parameters are given in Tables I and II, respectively. Note that many of the components are considered ideal as the focus of this work is not to evaluate component imperfections but rather to estimate the maximum achievable rate, i.e. the MI, of a coherent fiber system with transoceanic link length.

The leftmost block in Fig. 4 shows the polarization-division multiplexed (PDM) transmitter. After generating a pseudo-random binary sequence (PRBS), the bits are modulated. The resulting symbols are pulse-shaped in the digital domain with a root-raised cosine (RRC) filter with a roll-off factor of 0.05 and converted into the analog domain with an ideal digital-to-analog converter (DAC). The analog signal is transferred into the optical domain using an ideal push-pull Mach-Zehnder modulator (MZM) with an ideal laser. The number of co-propagating WDM channels, which are decorrelated copies of the central channel, is varied with the WDM spacing such that the overall occupied bandwidth is as close as possible to  $9 \cdot 50 = 450$  GHz while keeping the spectrum symmetrical around the center channel. This is to ensure that the channel of interest experiences approximately the same amount of nonlinearities during propagation, independent from the number of simulated channels. The relationship between channel spacing and number is shown vertically in the last two rows of Table I. The above steps are repeated to generate the signal of the y-polarization. Lastly, the two polarizations are added and the signal is launched into the fiber.

The dual-polarization signal propagates over 60 spans of single-mode fiber (SMF), each followed by an Erbium-doped fiber amplifier (EDFA). The total transmission distance is

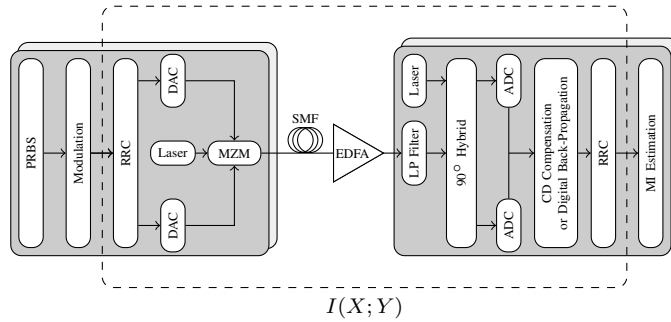


Fig. 4. Simulation setup of the examined optical communication system. The dashed box includes all components and subsystems that influence  $I(X; Y)$ .

6000 km with no inline dispersion compensation. Fiber propagation is simulated by solving the nonlinear Schrödinger equation numerically using the split-step Fourier method (SSFM) [34] with 32 samples per symbol (SpS).

The rightmost block in Fig. 4 shows the coherent receiver. The central WDM channel is extracted with an ideal band-pass filter whose bandwidth equals the WDM spacing. The incoming optical signal is mixed with a local oscillator laser with zero linewidth and no frequency offset in a  $90^\circ$  optical hybrid such that the in-phase and quadrature component of both polarizations are each made available to an ideal ADC and then jointly to the digital signal processing (DSP) sub-routines with 32 SpS. The DSP consists of ideal compensation of all chromatic dispersion (CD) that is accumulated during propagation. For our simulation layout, equalization to counteract intersymbol interference is not required because there is no polarization-mode dispersion (PMD) on the fiber and the Nyquist criterion is fulfilled by the RRC filters at transmitter and receiver. For one set of simulations, ideal single-channel DBP is performed, undoing both linear and nonlinear fiber effects. Carrier phase recovery (CPR) is not required because the lasers on the transmitter and receiver side are ideal and do not create phase perturbations. After matched RRC filtering and downsampling, the MI is calculated per polarization as outlined in Section III-B and then averaged over both polarizations.

The dashed box surrounding most of the simulation blocks in Fig. 4 depicts the channel for which the MI is determined. Note that not only the fiber itself is part of the channel but also components and algorithms on both the transmitter and receiver side. Hence, the influence of these algorithms has an impact on the MI and thus, on the net achievable data rate of the communication system.

### B. Simulation Results

For the outlined simulation setup, QAM of order 4, 16, and 64 is compared in terms of the respective MI. Additionally, the impact of ideal single-channel DBP is examined for 16-QAM and 64-QAM, and the spectral efficiency (SE) is analyzed for different WDM spacings.

1) *Different modulation schemes:* In Fig. 5, the MI per polarization is depicted over the launch power per channel in increments of 1 dBm. The curve for each modulation scheme follows the behavior that is typical for a nonlinear fiber system.

In the low-power regime, the performance is limited by noise originating from the optical amplifiers. The maximum MI is obtained at a power of  $-1$  dBm for all modulations. This is in agreement with [35] where it is analytically shown that the optimum launch power is constant for rectangular QAM of identical symbol rate. Beyond  $-1$  dBm, the impact of the nonlinearities becomes larger and reduces MI. Previous results obtained by considering an HD code and  $BER_{in}$  as figure of merit show a similar shape [36]. We will now discuss in more detail the maximum MI of 3.1 bits/symbol for 16-QAM obtained at the optimum launch power of  $-1$  dBm. This

TABLE I  
TRANSMISSION PARAMETERS

PRBS	2 <sup>18</sup> bits per polarization					
Modulation	{4, 16, 64}-QAM					
PDM	yes (independently)					
Baud rate	28 GBaud					
Data rate w/o FEC	{112, 224, 336} Gbit/s					
Pulse shaping	RRC					
Roll-off	0.05					
DAC/ADC resolution	$\infty$ (ideal)					
Laser linewidth	0 (ideal laser)					
MZM	ideal push-pull					
Power per channel	$-8$ dBm to 4 dBm					
WDM spacing [GHz]	50	45	40	35	30	27.5
WDM channels	9	11	11	13	15	17

TABLE II  
FIBER PARAMETERS

Fiber type	SMF
Carrier wavelength	1550 nm
Length per span	100 km
Number of spans	60
Attenuation $\alpha$	0.2 $\frac{\text{dB}}{\text{km}}$
Nonlinear coefficient $\gamma$	1.3 $\frac{1}{\text{W}\cdot\text{km}}$
Chromatic dispersion	17 $\frac{\text{ps}}{\text{nm}\cdot\text{km}}$
Dispersion slope	0
PMD	0
SSFM step size	0.1 km
SpS	32
EDFA noise figure	4 dB

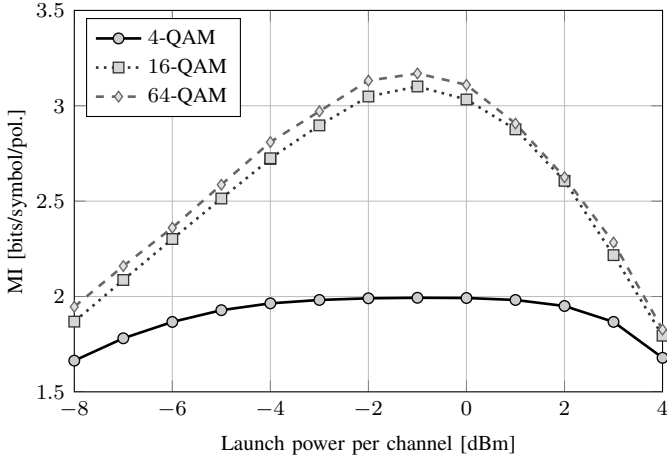


Fig. 5. MI over launch power per channel for QAM of order 4, 16, 64.

equals a net channel data rate of 174 Gbit/s in comparison to 100 Gbit/s of commercially available link based on QPSK. We know from Section II-B that MI is the achievable rate of transmission. Out of every  $\log_2(M) = 4$  bits per 16-QAM symbol, up to 3.1 bits can carry information and at least 0.9 bits must be reserved for the redundancy of the assumed ideal coding scheme. The maximum rate  $R$  that can be used while still achieving an arbitrarily small BER equals  $\frac{3.1}{\log_2(16)} \simeq 0.78$ . Consequently, any code with  $R > 0.78$  will inevitably lead to a significant, i.e. not arbitrarily small  $\text{BER}_{\text{out}}$  if the channel memory is neglected. An identical line of argument can be made for QPSK and 64-QAM. At the optimum launch power,  $R = \frac{1.99}{\log_2(4)} \simeq 0.99$  for QPSK and  $R = \frac{3.17}{\log_2(64)} \simeq 0.53$  for 64-QAM. Clearly, QPSK is a suboptimal choice of modulation because it only achieves 1.99 bits/symbol while more than one additional bit of information per symbol is available by using 16-QAM. Fig. 1 also provides a hint that a higher modulation than QPSK should be used for the considered long-haul link. Assume that the optical system operates at the optimal launch power of  $-1$  dBm. The 1.99 bits/symbol achieved by QPSK at this power correspond to about 10 dB SNR for a hypothetical equivalent AWGN channel. At 10 dB SNR, we could get to 3.16 bits/symbol by using 16-QAM and still have an arbitrarily small BER. Consequently, we prefer 16-QAM to QPSK for an AWGN channel as well as for the outlined optical fiber system with nonlinearities.

Comparing the two highest-order modulation schemes in Fig. 5, 64-QAM slightly outperforms 16-QAM over the entire range of launch powers. At the optimum launch power, the respective MIs differ by less than 0.1 bits/symbol. In order to make use of this little gain, a channel code of smaller rate is required for higher modulations. Also, the increased number of constellation levels imposes higher requirements on components such as the ADC and DAC or on the laser linewidth, and also on DSP algorithms such as CPR. We argue that for the simulation setup of Section IV-A with a transoceanic SMF link, 16-QAM is the modulation format that offers the best tradeoff between MI and complexity. Resorting again to Fig. 1 as an illustration and assuming that

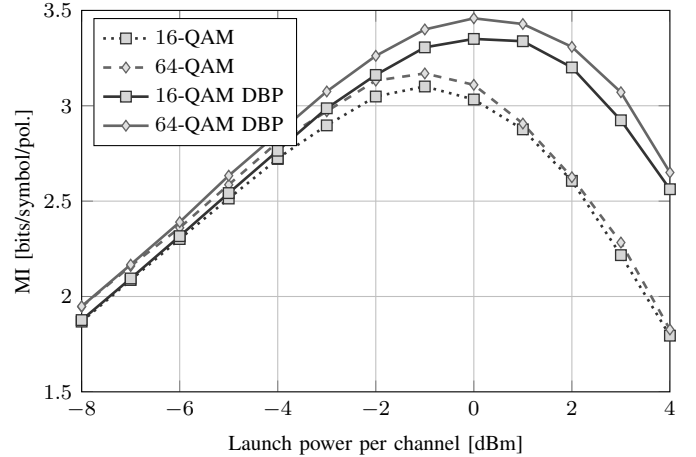


Fig. 6. The effect of ideal single-channel DBP for 16-QAM and 64-QAM after 6000 km of transmission.

we operate in an equivalent AWGN channel, there is only about 0.1 bits/symbol to be gained by using 64-QAM instead of 16-QAM at an SNR of 10 dB. This supports our result that 16-QAM is the best choice for our long-haul simulation setup. This is in agreement with experimental results [37] where for 5000 km SMF and higher EDFA noise figures, using a modulation format with more than 16 states does not result in a notable gain.

One might argue that four-dimensional (4D) modulations based on set-partitioning (SP) [38] have shown better performance than modulating each polarization independently. Experiments [39] suggest that SP-128-QAM [40] can outperform dual-polarization (DP)-16-QAM by 1.9 dB SNR at a  $\text{BER}_{\text{in}}$  of  $10^{-3}$  and identical net bit rate. This comparison, however, is biased because SP-128-QAM is essentially DP-16-QAM with an inherent single parity check (SPC) code of rate  $R = \frac{\log_2(M)-1}{\log_2(M)} = \frac{7}{8}$  applied such that the Euclidean distance between neighboring symbols in the 4D constellation space is increased. With such a coding scheme in place, SP-128-QAM clearly must be better than uncoded DP-16-QAM. However, SPC is not ideal in terms of coding performance but its strength rather lies in the very low complexity. Accordingly, better performance is achieved if an ideal code of rate  $\frac{7}{8}$  instead of the SPC is used. SP-128-QAM as DP-16-QAM with an inherent low-performance low-complexity code is hence not treated in this work as we focus on the maximum achievable rate. The same argument holds for schemes of different orders that are also based on SP.

2) *Digital back-propagation*: In the following, DBP is analyzed as an example of the impact of a particular DSP algorithm on the achievable rate. DBP is a powerful yet complex approach to mitigate the nonlinear signal interactions by back-propagating the signal in the digital domain at the receiver [41, Sec. 2]. We perform ideal single-channel DBP with a step size that is identical to the one used for the SSFM and also with identical SpS. The results are shown in Fig. 6 for QAM of order 16 and 64, and a WDM spacing of 50 GHz. All other parameters are as presented in Section IV-A. The maximum MI is obtained at 0 dBm launch power instead of  $-1$  dBm

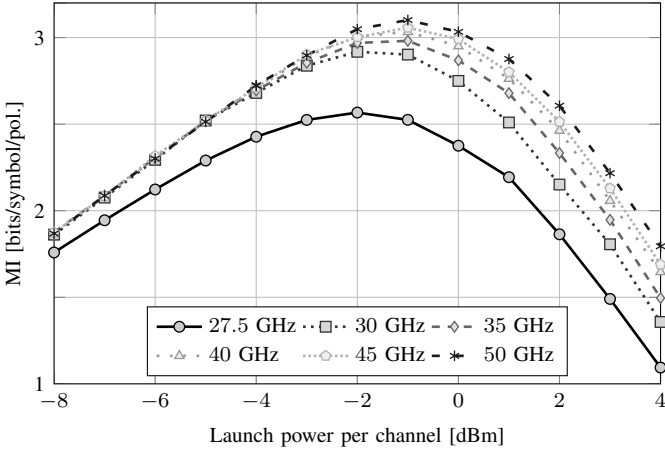


Fig. 7. MI over power per channel for varying WDM spacings and 16-QAM.

without DBP as the amount of nonlinearities is effectively reduced by DBP. The maximum MI is 3.35 bits/symbol for 16-QAM and 3.45 bits/symbol for 64-QAM, which corresponds to an increase by 0.25 bits/symbol and 0.28 bits/symbol, respectively, compared to the case without DBP. As both step size and SpS are identical to the SSFM, this is the maximum gain possible by deterministic single-channel DBP for the presented simulation setup.

3) *WDM spacings*: In Fig. 7, MI is depicted for varying launch powers, WDM spacings from 27.5 GHz to 50 GHz, and without DBP. The number of co-propagating channels is varied according to Table I. Decreasing the spacing from 50 GHz to 30 GHz does not affect MI in the linear regime. Once the launch power is increased such that the system is driven into the nonlinear regime, MI declines with decreasing channel spacing. For 30 GHz, 2.9 bits/symbol are achievable. While this behavior is qualitatively expected as the phase mismatch between co-propagating signals increases with spectral spacing and hence the impact of four-wave mixing decreases [42, Sec. 10.1], it is interesting to consider it quantitatively. A decrease in channel spacing by 60% leads to a drop in MI of only about 6.5%, from 3.1 bits/symbol to 2.9 bits/symbol. If the channel spacing is further reduced to 27.5 GHz, the MI significantly decreases not only for high launch powers but also in the linear regime. The channel spacing is in this case smaller than the  $28 \cdot 1.05 = 29.4$  GHz occupied by the signal. As the interference due to this spectral overlap is essentially noise, the optical signal is subject to additional impairments and the MI decreases.

Most of the MI curves in Fig. 7 are close to each other, yet the channel spacings differ a lot. This leads to investigate SE, shown in Fig. 8. Note that net SE is depicted, i.e. coding overhead for an ideal FEC scheme is taken into account and an arbitrarily small BER is achievable by such a code. A maximum DP SE of 5.7 bits/s/Hz is obtained for a WDM spacing of 30 GHz. For this spacing almost the entire available spectrum is used, which more than compensates for the slightly smaller MI found in Fig. 7. To put this SE into perspective, it is by 0.7 bit/s/Hz larger than the 5 bits/s/Hz SE that has been achieved experimentally over 6600 km pure-

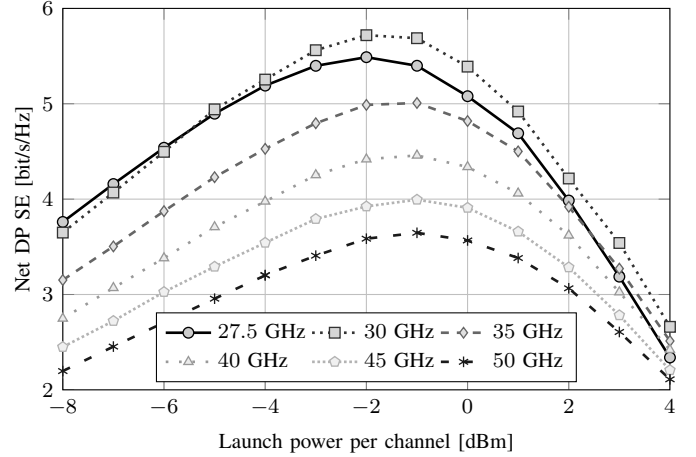


Fig. 8. Net DP SE over power per channel for varying WDM spacings and 16-QAM.

silica fiber core fiber and a hybrid EDFA-Raman amplification scheme [8].

SE in general decreases with increasing channel spacing as long as the WDM spacing is larger than the bandwidth occupied by the signal. Somewhat surprisingly, 27.5 GHz gives the highest SE in the linear regime up to  $-4$  dBm and performs well also for high launch powers. This behavior, however, is expected to vanish if an optical network with add-drop multiplexers is considered. The repeated filtering in combination with the spectral broadening of the pulse will further deteriorate the MI for a fiber system with sub-Nyquist WDM spacing.

## V. CONCLUSION

In this work, we estimate MI by means of histograms for which a method to find the correct bin number is presented. A simplified channel model for the optical fiber channel is used to show the accuracy of our MI estimation method. The method is applied to a coherent optical fiber system with 6000 km of standard fiber and the MI estimate is used as both an absolute and relative figure of merit. For ideal transmitter and receiver components yet without DBP, 16-QAM proves to be the modulation format that offers the best tradeoff between complexity and data rate for transoceanic distances. An MI of 3.1 bits/symbol is achievable for 16-QAM and a 50 GHz spacing. This means that any FEC for the considered system must have an overhead of at least 29% if memory from the channel is not considered. The amount of memory in an optical fiber system and how to make use of it remain open interesting questions as they may lead to a further increase in data rate. MI also allows to relatively quantify the impact of receiver subsystems. Using ideal single-channel DBP as an example, a respective maximum gain of 0.25 bits/symbol for 16-QAM and 0.28 bits/symbol for 64-QAM is achieved with only the center channel back-propagated. By extending this to more channels, the impact of nonlinear interchannel interactions and also the impact of nonlinear signal-noise interactions can be quantified. When the WDM channel spacing is decreased to almost the signal bandwidth, a maximum SE of 5.7 bits/s/Hz over both



polarizations is possible. While this value can be further increased by employing a scheme to mitigate fiber nonlinearities, it is questionable whether the potential increase in data rate is sufficient to cater for future capacity requirements.

The presented analysis is applicable to any component or method employed between the modulator on the transmitter side and the decoder input at the receiver in order to quantify the potential data rate gain or loss of a subsystem. For example, data-aided equalization can be compared to blind equalization as to the achievable rate decreased by the training symbols. Also, the effect of upgrading to more advanced amplification schemes or fibers can be quantified.

## REFERENCES

- [1] A. Chraplyvy, "The coming capacity crunch," in *Proc. European Conference on Optical Communication (ECOC)*, Paper Mo.1.0.2, 2009.
- [2] P. J. Winzer, "Spatial multiplexing: The next frontier in network capacity scaling," in *Proc. European Conference on Optical Communication (ECOC)*, Paper We.1.D.1, 2013.
- [3] C. E. Shannon, "A mathematical theory of communication," *Bell Labs Techn. J.*, vol. 27, pp. 379–423 and 623–656, Jul. 1948.
- [4] P. P. Mitra and J. B. Stark, "Nonlinear limits to the information capacity of optical fibre communications," *Nature*, vol. 411, no. 6841, pp. 1027–1030, Jun. 2001.
- [5] R.-J. Essiambre, G. Kramer, P. J. Winzer, G. J. Foschini, and B. Goebel, "Capacity limits of optical fiber networks," *J. Lightw. Technol.*, vol. 28, no. 4, pp. 662–701, Feb. 2010.
- [6] A. Leven, F. Vacondio, L. Schmalen, S. ten Brink, and W. Idler, "Estimation of soft FEC performance in optical transmission experiments," *IEEE Photon. Technol. Lett.*, vol. 23, no. 20, pp. 1547–1549, Oct. 2011.
- [7] T. Fehenberger and N. Hanik, "Information quality (IQ) factor as soft-decision decoding threshold for optical communications," in *Proc. European Conference on Optical Communication (ECOC)*, P.4.12, 2013.
- [8] M. Salsi, R. Rios-Muller, J. Renaudier, P. Tran, L. Schmalen, A. Ghazisaeidi, H. Mardoyan, P. Brindel, G. Charlet, and S. Bigo, "38.75 Tb/s transmission experiment over transoceanic distance," in *Proc. European Conference on Optical Communication (ECOC)*, Paper PD3.E.2, 2013.
- [9] J. Cho, C. Xie, and P. J. Winzer, "Analysis of soft-decision FEC on non-AWGN channels," *Opt. Express*, vol. 20, no. 7, pp. 7915–7928, Mar. 2012.
- [10] R. Koetter and A. Vardy, "Algebraic soft-decision decoding of Reed-Solomon codes," *IEEE Trans. Inf. Theory*, vol. 49, no. 11, pp. 2809–2825, Nov. 2003.
- [11] J. G. Proakis and M. Salehi, *Digital Communications*, 5th ed. New York, USA: McGraw-Hill, 2008.
- [12] ITU, *Recommendation G.975: Forward error correction for submarine systems*, Oct. 2000.
- [13] —, *Recommendation G.975.1: Forward error correction for high bit-rate DWDM submarine systems*, Feb. 2004.
- [14] B. P. Smith, A. Farhood, A. Hunt, F. R. Kschischang, and J. Lodge, "Staircase codes: FEC for 100 Gb/s OTN," *J. Lightw. Technol.*, vol. 30, no. 1, pp. 110–117, Jan. 2012.
- [15] S. Kudekar, T. Richardson, and R. L. Urbanke, "Spatially coupled ensembles universally achieve capacity under belief propagation," *IEEE Trans. Inf. Theory*, vol. 59, no. 12, pp. 7761–7813, Dec. 2013.
- [16] E. Arıkan, "Channel polarization: A method for constructing capacity-achieving codes for symmetric binary-input memoryless channels," *IEEE Trans. Inf. Theory*, vol. 55, no. 7, pp. 3051–3073, Jul. 2009.
- [17] T. M. Cover and J. A. Thomas, *Elements of Information Theory*, 2nd ed. New Jersey, USA: Wiley-Interscience, 2006.
- [18] L. Hanzo, S. X. Ng, T. Keller, and W. Webb, *Quadrature Amplitude Modulation*, 2nd ed. West Sussex, UK: IEEE Press, 2004.
- [19] D. Arnold, H.-A. Loeliger, P. Vontobel, A. Kavcic, and W. Zeng, "Simulation-based computation of information rates for channels with memory," *IEEE Trans. Inf. Theory*, vol. 52, no. 8, pp. 3498–3508, Aug. 2006.
- [20] P. Poggiolini, "The GN model of non-linear propagation in uncompensated coherent optical systems," *J. Lightw. Technol.*, vol. 30, no. 24, pp. 3857–3879, Dec. 2012.
- [21] B. Goebel, R.-J. Essiambre, G. Kramer, P. J. Winzer, and N. Hanik, "Calculation of mutual information for partially coherent Gaussian channels with applications to fiber optics," *IEEE Trans. Inf. Theory*, vol. 57, no. 9, pp. 5720–5736, Sep. 2011.
- [22] P. Leoni, S. Calabrò, and B. Lankl, "Constellation expansion for 100G transmission," *IEEE Photon. Technol. Lett.*, vol. 25, no. 19, pp. 1904–1907, Oct. 2013.
- [23] C. Daub, R. Steuer, J. Selbig, and S. Kloska, "Estimating mutual information using b-spline functions - an improved similarity measure for analysing gene expression data," *BMC Bioinformatics*, vol. 5, Aug. 2004.
- [24] L. Paninski, "Estimation of entropy and mutual information," *Neural Computation*, vol. 15, no. 6, pp. 1191–1253, Jun. 2003.
- [25] Y. Moon, B. Rajagopalan, and U. Lall, "Estimation of mutual information using kernel density estimators," *Physical Review E*, vol. 52, no. 3, pp. 2318 – 2321, Sep. 1995.
- [26] A. Alvarado, F. Brännström, and E. Agrell, "High snr bounds for the bicm capacity," in *IEEE Information Theory Workshop (ITW)*, Oct 2011, pp. 360–364.
- [27] B. Goebel, Z. Dawy, J. Hagenauer, and J. Mueller, "An approximation to the distribution of finite sample size mutual information estimates," in *International Conference on Communications (ICC)*, vol. 2, May 2005, pp. 1102–1106.
- [28] A. Kraskov, H. Stögbauer, and P. Grassberger, "Estimating mutual information," *Phys. Rev. E*, vol. 69, p. 066138, Jun. 2004.
- [29] G. A. Darbellay and I. Vajda, "Estimation of the information by an adaptive partitioning of the observation space," *IEEE Trans. Inf. Theory*, vol. 45, no. 4, pp. 1315–1321, May 1999.
- [30] D. W. Scott, "On optimal and data-based histograms," *Biometrika*, vol. 66, no. 3, pp. 605–610, 1979.
- [31] H. Shimazaki and S. Shinomoto, "A method for selecting the bin size of a time histogram," *Neural Computation*, vol. 19, no. 6, pp. 1503–1527, Jun. 2007.
- [32] K. Knuth, "Optimal data-based binning for histograms," *arXiv:physics/0605197v2*, Sep. 2013.
- [33] G. Ungerboeck, "Channel coding with multilevel/phase signals," *IEEE Trans. Inf. Theory*, vol. IT-28, no. 1, pp. 55–67, Jan. 1982.
- [34] O. Sinkin, R. Holzlohner, J. Zweck, and C. Menyuk, "Optimization of the split-step Fourier method in modeling optical-fiber communications systems," *J. Lightw. Technol.*, vol. 21, no. 1, pp. 61–68, Jan. 2003.
- [35] K. Kikuchi, "Analyses of wavelength- and polarization-division multiplexed transmission characteristics of optical quadrature-amplitude-modulation signals," *Opt. Express*, vol. 19, no. 19, pp. 17985–17995, Sep. 2011.
- [36] S. Kilmurray, T. Fehenberger, P. Bayvel, and R. Killey, "Comparison of the nonlinear transmission performance of quasi-Nyquist WDM and reduced guard interval OFDM," *Opt. Express*, vol. 20, no. 4, pp. 4198–4205, Feb. 2012.
- [37] I. B. Djordjevic, H. G. Batshon, L. Xu, and T. Wang, "Coded polarization-multiplexed iterative polar modulation (PM-IPM) for beyond 400 Gb/s serial optical transmission," in *Proc. Optical Fiber Communication Conference (OFC)*, Paper OMK2, 2010.
- [38] E. Agrell and M. Karlsson, "Power-efficient modulation formats in coherent transmission systems," *J. Lightw. Technol.*, vol. 27, no. 22, pp. 5115–5126, Nov. 2009.
- [39] T. A. Eriksson, M. Sjödin, P. Johannisson, P. A. Andrekson, and M. Karlsson, "Comparison of 128-SP-QAM and PM-16QAM in long-haul WDM transmission," *Opt. Express*, vol. 21, no. 16, pp. 19269–19279, Aug. 2013.
- [40] L. Coelho and N. Hanik, "Global optimization of fiber-optic communication systems using four-dimensional modulation formats," in *Proc. European Conference on Optical Communication (ECOC)*, Paper Mo.2.B.4, 2011.
- [41] X. Li, X. Chen, G. Goldfarb, E. Mateo, I. Kim, F. Yaman, and G. Li, "Electronic post-compensation of WDM transmission impairments using coherent detection and digital signal processing," *Opt. Express*, vol. 16, no. 2, pp. 880–888, Jan. 2008.
- [42] G. P. Agrawal, *Nonlinear Fiber Optics*, 4th ed. London, UK: Academic Press, 2007.